Role of surface crossings in the photochemistry of nitromethane

Juan F. Arenas, Juan C. Otero, Daniel Peláez, and Juan Soto
Department of Physical Chemistry, Faculty of Sciences, University of Málaga, E-29071 Málaga, Spain

(Received 14 September 2004; accepted 3 December 2004; published online 23 February 2005)

The photodissociation dynamics of nitromethane (CH_3NO_2) starting at the S_3 excited state has been studied at the complete active space self-consistent field level of theory in conjunction with atomic natural orbital type basis sets. In addition, the energies of all the critical points and the energy profiles connecting them have been recomputed with the multiconfigurational second-order perturbation method. It is found that the key step in the reaction mechanism is a radiationless decay through an S_3/S_2 conical intersection. The branching space spanned by the gradient difference and nonadiabatic coupling vectors of this crossing point comprises dissociation into excited nitromethane plus singlet atomic oxygen [$CH_3NO(1A'')+O(^1D)$] and $S_3 \rightarrow S_2$ deactivation, respectively. Furthermore, deactivated nitromethane $S_{n\ (n<3)}$ can decompose in subsequent steps into CH_3+NO_2, where NO_2 is generated at least in two different electronic states ($1\ ^2B_2$ and $1\ ^2A_1$). It is shown that formation of excited nitric oxide NO($A\ ^2\Sigma$) arises from $CH_3NO(1A'')$ generated in the previous step. In addition, four crossings between singlet and triplet states are localized; however, no evidence is found for a relevant role of such crossings in the photochemistry of CH_3NO_2 initiated at S_3 state in the gas phase. © *2005 American Institute of Physics*.
[DOI: 10.1063/1.1851977]

I. INTRODUCTION

Nitromethane (CH_3NO_2) is the simplest member of the nitro-compound family. Its structural simplicity contrasts to the rich chemistry exhibited on both the ground and excited electronic states. For this reason, it is very attractive for mechanistic studies and is indeed a very well-studied system from both the experimental and theoretical points of view.

Although the main motivation to study this molecule has arisen from the fact that it is an important prototypical energetic material,[1–3] the understanding of its chemistry is relevant in other fields such as atmospheric chemistry or biochemistry. For example, nitroglycerin is used for cardiovascular therapy since the very beginning of its discovery, however, the biochemical decomposition mechanism of this compound is not yet well known.[4] So that, a detailed knowledge of the chemistry of nitromethane should become of great assistance in understanding the biochemistry of this molecule.

The absorption spectrum[5] of nitromethane consists of a strong band centered around 6.25 eV which extends over the 5.5–7.5 eV range, and a much weaker one ranging from 3.5 to 5.0 eV with an absorption maximum around 4.59 eV. These maxima have been assigned[6] to $\pi(\mathrm{NO}) \rightarrow \pi^*(\mathrm{NO})$ and $\sigma(\mathrm{CN}) \rightarrow \pi^*(\mathrm{NO})$ transitions, respectively. The primary photolytic process at either of these absorption wavelengths is cleavage of the C–N bond to yield CH_3 and NO_2 [Eq. (1)]:

$$CH_3NO_2 + h\nu \rightarrow CH_3 + NO_2. \quad (1)$$

Concerning the photochemistry of nitromethane, there have been a number of studies using different wavelengths for the study of its photodissociation dynamics. The results vary widely in their findings, and up to date no clear picture of the dissociation pathways has emerged.[1] Below, we briefly discuss some of these works.

The experimental works of Butler *et al.*,[7] Blais,[8] Lao *et al.*,[9] and Moss, Trentelman, and Houston[10] all at 193 nm support Eq. (1) as the primary reaction and propose at least two channels by which CH_3 and NO_2 are generated. Moss, Trentelman, and Houston[10] suggested the following mechanism:

a. Major channel.

$$CH_3NO_2 + h\nu(193\ \mathrm{nm}) \rightarrow CH_3 + NO_2(1\ ^2B_2) \rightarrow CH_3 + NO(X\ ^2\Pi) + O(^3P). \quad (1a)$$

b. Minor channel.

$$CH_3NO_2 + h\nu(193\ \mathrm{nm}) \rightarrow CH_3 + NO_2(2\ ^2B_2) \xrightarrow{h\nu} CH_3 + NO(A\ ^2\Sigma^+) + O(^3P). \quad (1b)$$

The experimental observations on the 193 nm photolysis of nitromethane are summarized as follows:[10] (i) The observed translational energy distributions of methyl radical are indicative of two dissociation pathways. (ii) The internal excitation energy of the methyl fragment is observed to be rather modest. (iii) The secondary dissociation products of the major channel [Eq. (1a), NO($X\ ^2\Pi$) and O(^3P)] have a distribution of internal and translational energy consistent with a dissociation on a repulsive surface. (iv) Electronically excited NO($A\ ^2\Sigma^+$) is found to be a secondary product of the minor channel, Eq. (1b), a product that requires absorption of two 193 nm photons. (v) Relatively little translational energy is released in the second decomposition step of the minor channel.

The decomposition following excitation via the long wavelength absorption leads to the production of vibrationally excited NO_2 in its electronic ground state ($^2A_1$) (Refs. 11 and 12) along with small quantities of it in an unidentified excited electronic state.[12] It is not confirmed the

formation of other reaction products such as OH radicals. While Zabarnick, Fleming, and Baronavski[13] detected a small yield of OH in the collision free photodissociation of CH_3NO_2 at 266 nm, Greenblatt, Zuckermann, and Hass[14] did not find any evidence of OH formation from photolysis of nitromethane at 282 nm. In addition, Rajchenbach, Jonusauskas, and Rullière[15] observed an important nonradiative deexcitation channel in the photolysis of liquid nitromethane at 299 nm, using subpicosecond time-resolved coherent antistokes Raman spectroscopy experiments.

There is also evidence of minor competing processes [Eqs. (2) and (3)]:[16–19]

$$CH_3NO_2 + h\nu \rightarrow CH_3NO + O, \tag{2}$$

$$CH_3NO_2 + h\nu \rightarrow CH_2O + HNO. \tag{3}$$

The reaction paths of the low-lying singlet and triplet states of nitromethane, which lead to dissociation into CH_3 and NO_2, have been recently studied by ourselves[6] at the multiconfigurational second-order perturbation theory MS-CASPT2 level. It was demonstrated that at excitation energies under 198 nm, only valence states are involved in the photodissociation dynamics. Therefore, it was possible to determine reliable energy barriers for cleavage of the C–N bond in each valence state by using standard basis sets. The aim of the present work is to explore the potential energy surfaces (singlet and triplet) in the neighborhood of the Franck–Condon regions. In these domains of the potential energy surfaces, there are several surface crossings (conical intersections and intersystem crossings) which are of relevant importance in the dissociation dynamics of nitromethane at 193 nm.

II. METHODS OF CALCULATION

Generally contracted basis sets of atomic natural orbital (ANO) type obtained from C, N, O(14*s*9*p*4d3f)/H(8*s*4*p*3*d*) primitive sets,[20] the so-called ANO-L basis sets, with the C,N,O[4*s*3*p*2*d*1*f*]/H[3*s*2*p*1*d*] contraction schemes were used in all of the geometry optimizations of the relevant species involved in the photolysis of nitromethane, which were performed at the complete active space self-consistent field (CASSCF) (Ref. 21) level of theory as implemented in the MOLCAS 5.4 program.[22] On the other hand, the localization of the crossing points (conical intersections and intersystem crossings) were done with the algorithm implemented in the GAUSSIAN program[23(a)] by Bearpark, Robb, and Schlegel,[23(b)] that is, the gradient difference and nonadiabatic coupling vectors are computed using state average orbitals in the manner suggested by Yarkony.[23(c)] Although this procedure requires the computation of the Hessian at each iteration, the contributions that arise from the derivatives of the orbital rotations have been neglected.[23(b)]

The electronic configuration of the ground state is given by

$$1a'^2 1a''^2 2a'^2 3a'^2 4a'^2 2a''^2 5a'^2 6a'^2 7a'^2 8a'^2 3a''^2 4a''^2 9a'^2 5a''^2 10a'^2 6a''^2,$$

which corresponds with the following assignment of the molecular orbitals

$$\cdots\sigma(\mathrm{CH}), 2\mathrm{s(N)}, \sigma(\mathrm{NO}), \pi(\mathrm{NO}), \sigma(\mathrm{NO}), \sigma(\mathrm{CH}), \sigma(\mathrm{CH}),$$

$$\mathrm{n}\sigma(\mathrm{O}), \sigma(\mathrm{CN}), \mathrm{n}\pi(\mathrm{O}),$$

where $\cdots$ designates the six doubly occupied *s*-type molecular orbitals. The active space is built from this reference configuration by distributing fourteen electrons in eleven orbitals, that is, the valence orbitals with exception of the σ(CH)-type ones are optimized.[6,24,25]

The stationary points (minima and saddle points) were characterized by their CASSCF analytic harmonic vibrational frequencies computed by diagonalizing the mass-weighted Cartesian force constant matrix, i.e., the Hessian matrix $\boldsymbol{H}$. In order to perform the vibrational analysis of nonstationary points, such as vertical excitations, the eigenvectors corresponding to rotations, translations, and gradient were projected out of the Hessian matrix as described in a previous paper.[26]

The energies of all of the critical points have been recomputed with the multistate extension of the MS-CASPT2.[27] Therefore, the CASSCF wave functions were used as reference in the second-order perturbation treatment, keeping frozen the 1*s* electrons of the carbon, oxygen, and nitrogen atoms, respectively, as determined in the SCF calculations. To minimize the contamination of the pertubated wave function by intruder states, the technique of the imaginary level shift[28] has been introduced in all of the recomputed energies.

The transition dipole moments were computed according to the CAS state interaction procedure[29] in conjunction with the perturbatively modified CAS reference functions obtained as linear combinations of all the states involved in the MS-CASPT2 calculation.

The spin–orbit coupling constants, which are the matrix elements that represent the coupling between two states of different multiplicity,

$$\langle \mathbf{H}_{\mathrm{SO}} \rangle^{\mathrm{I,J}} = \left\langle {}^{\mathrm{I}}\Psi(M_S) \middle| H_{\mathrm{SO}} \middle| {}^{\mathrm{J}}\Psi(M_{s'}) \right\rangle \tag{4}$$

have been computed by using an effective one-electron Fock-type spin–orbit Hamiltonian, as suggested by Hess and co-workers[30] and with the RASSI program implemented in MOLCAS 5.4; $({}^{\mathrm{I}}\Psi(M_S)$ is the wave function including the spin state and M_S is the component of one sublevel). To avoid the

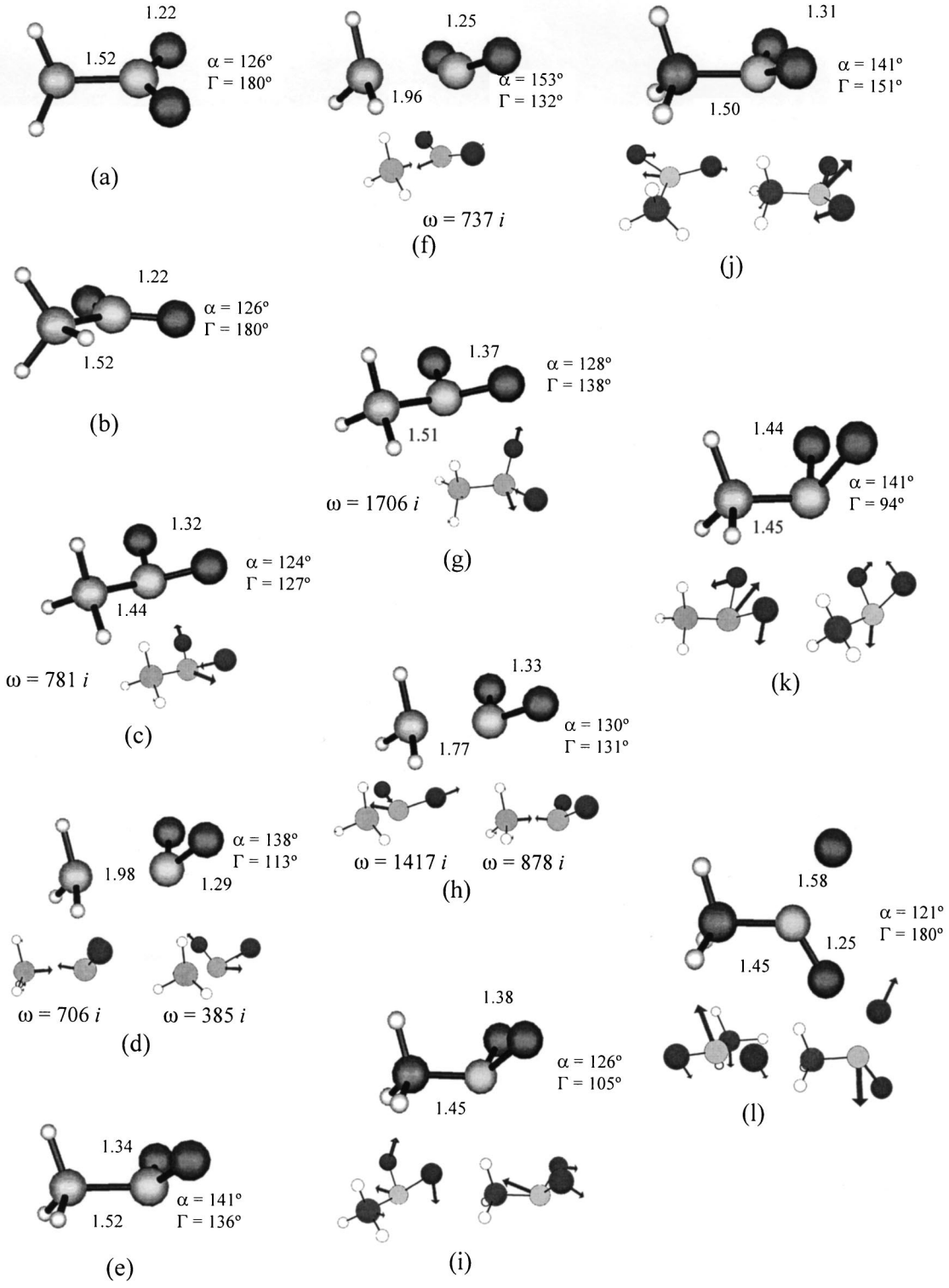

FIG. 1. Geometries of the critical points of nitromethane localized on the singlet surfaces at the CAS (14,11)/ANO-L level; conical intersections calculated at the CAS(14,10)/6-31G* level. The arrows in the lower structures correspond to imaginary modes (for stationary points) or nonadiabatic coupling (left) and gradient difference (right) vectors (for conical intersections). (a) S_0, $1\,^1A'$ staggered minimum; (b) S_0, $1\,^1A'$ eclipsed minimum; (c) S_1, $1\,^1A''$ first-order saddle point; (d) S_1, $1\,^1A''$ transition state for dissociation into CH_3+NO_2 ($1B_2$); (e) S_2, $2\,^1A'$ minimum; (f) S_2, $2\,^1A'$ transition state for dissociation into CH_3+NO_2 ($1B_1$); (g) S_3, $2\,^1A''$ first-order saddle point; (h) S_2, $2\,^1A''$ transition state for dissociation into CH_3+NO_2 ($1A_2$); (i) S_1/S_0 conical intersection; (j) S_2/S_1 conical intersection; (k) S_2/S_1 (Ci3) conical intersection; and (l) S_3/S_2 conical intersection. Structures represented with the MACMOLPLT program (Ref. 42).

calculation of multicenter one- and two-electron integrals, the atomic mean field integrals have been used.[31] Spin–orbit coupling between configuration interaction (CI) eigenvectors of the effective Hamiltonian form a Hermitian matrix. Since the basis set is real and the spin–orbit coupling operator is complex, all spin–orbit coupling constants are off-diagonal. The diagonal elements are the CI energies without spin–orbit couplings. Diagonalizing this Hermitian matrix yields spin–orbit coupled states.[32] To estimate the spin–orbit coupling interaction between two states of different multiplicity, we

TABLE I. MS-CASPT2 energies of the critical points of nitromethane on the singlet surfaces. Zero point energy correction is included. Absolute reference energy, $E_h = -244.621\,23$ hartree.

Geometry	Configuration	ΔE (kcal/mol)	ZPE (kcal/mol)
M1a, S_0, $1\,^1A'$ [Fig. 1(a)]	$\cdots n\sigma(O)^2\sigma(CN)^2 n\pi(O)^2$	0.0 (0.00)[a]	3.2
Vt1, S_1, $1\,^1A''$[b]	$\cdots n\sigma(O)^1\pi^*(NO)^1$	91.5 (3.97)	3.0
Vt2, S_2, $2\,^1A'$[b]	$\cdots\sigma(CN)^1\pi^*(NO)^1$	99.0 (4.29)	3.0
Vt3, S_3, $2\,^1A''$[b]	$\cdots n\pi(O)^1\pi^*(NO)^1$	141.8 (6.15)	2.6
M1b, S_0, $1\,^1A'$ [Fig. 1(b)]	$\cdots n\sigma(O)^2\sigma(CN)^2 n\pi(O)^2$	0.0 (0.00)	3.2
Sd1, S_1, $1\,^1A''$ [Fig. 1(c)]	$\cdots n\sigma(O)^1\pi^*(NO)^1$	65.4 (2.84)	2.9
TS1, S_1, $1\,^1A''$ [Fig. 1(d)]	$\cdots n\sigma(O)^1\pi^*(NO)^1$	93.1 (4.04)	2.6
M2, S_2, $2\,^1A'$ [Fig. 1(e)]	$\cdots\sigma(CN)^1\pi^*(NO)^1$	83.4 (3.62)	3.1
TS2, S_2, $2\,^1A'$ [Fig. 1(f)]	$\cdots\sigma(CN)^1\pi^*(NO)^1$	104.0 (4.51)	2.8
Sd2, S_3, $2\,^1A''$ [Fig. 1(g)]	$\cdots n\pi(O)^1\pi^*(NO)^1$	117.0 (5.08)	2.9
TS3, S_3, $2\,^1A''$ [Fig. 1(h)]	$\cdots n\pi(O)^1\pi^*(NO)^1$	129.4 (5.61)	2.7
Ci1, S_1/S_0 [Fig. 1(i)][c]		73.4 (3.18)	…
Ci2, S_2/S_1 [Fig. 1(j)][c]		84.0 (3.64)	…
Ci3, S_2/S_1 [Fig. 1(k)][c]		101.4 (4.40)	…
Ci4, S_3/S_2 [Fig. 1(l)][c]		111.7 (4.84)	…
Dis0, S_0, CH_3+NO_2 ($1A_1$)		61.4 (2.66)	2.4
Dis1, S_1, CH_3+NO_2 ($1B_2$)		90.5 (3.92)	2.2
Dis2, S_2, CH_3+NO_2 ($1B_1$)		100.7 (4.37)	2.5
Dis3, S_3, CH_3+NO_2 ($1A_2$)		113.7 (4.93)	2.2
Dis4, S_2, CH_3NO ($1A''$)$+O(^1D)$		113.6 (4.93)	2.8
CH_3+NO_2 ($2B_2$)		160.2 (6.95)	2.3
CH_3+NO_2 ($2B_1$)		182.8 (7.93)	2.1

[a]In parenthesis energy in eV.
[b]Oscillator strength, $f=0.876\times10^{-4}$; $f=0.147\times10^{-5}$; $f=0.189$.
[c]Zero point energy correction not included.

have used the root mean squared coupling constant defined by Eq. (5),[33]

$$\mathrm{SOC}=\left(\sum_{M_s}\mathrm{Re}^2(\langle\hat{H}_{\mathrm{SO}}\rangle_{\mathrm{I,J},M_s})+\mathrm{Im}^2(\langle\hat{H}_{\mathrm{SO}}\rangle_{\mathrm{I,J},M_s})\right)^{1/2}. \quad (5)$$

III. RESULTS

A. Singlet potential energy surfaces and conical intersections

There are two isoenergetic minima of C_s symmetry on the ground state surface of nitromethane [staggered [M1a, Fig. 1(a)] and eclipsed [M1b, Fig. 1(b)]]. However, the staggered conformers are the only stationary arrangements on the excited surfaces (singlet and triplet). Furthermore, since the staggered isomers are computationally more convenient, in what follows the discussion will be based on the staggered structures. Above the ground state, three valence singlet states exist. On these excited surfaces the following stationary points have been localized: (i) on the S_1 (C_s) surface, a first-order saddle point [Sd1, Fig. 1(f)] which is the lowest energy point and a second-order saddle point [TS_1, Fig. 1(d)] which correlates adiabatically with the dissociation products CH_3 ($1\,^2A_1'$) and NO_2 ($1\,^2B_2$) [Dis1]; (ii) on the S_2 (C_s) surface, a minimum [M2, Fig. 1(e)] and a first-order saddle point [TS_2, Fig. 1(d)] which is the transition state for dissociation into CH_3 ($1\,^2A_1'$) and NO_2 ($1\,^2B_1$) [Dis2]; and (iii) on the S_3 (C_s) surface, a first-order saddle point [Sd2, Fig. 1(g)] and a second-order saddle point [TS_3, Fig. 1(h)] which correlates adiabatically with the dissociation products CH_3 ($1\,^2A_1'$) and NO_2 ($1\,^2A_2$) [Dis3]. The MS-CASPT2 energies of all these structures along with the vertical transitions are collected in Table I.

In addition, the following surface crossings (conical intersections) have been localized: (a) S_1/S_0 conical intersection [Ci1, Fig. 1(i)]; (b) S_2/S_1 conical intersection [Ci2, Fig. 1(j)]; (c) S_2/S_1 conical intersection [Ci3, Fig. 1(k)]; and (d) S_3/S_2 conical intersection [Ci4, Fig. 1(l)]. The geometries of these crossing points have been optimized as the lowest energy points in the seam of crossing of two singlet surfaces. The energy profiles running from the geometry of the S_0 minimum (Franck–Condon point) to each of these conical intersections (Ci1, Ci2, and Ci3) are represented in Fig. 2. Such interpolations have been computed at the MS-CASPT2 level. In order to build these curves, an interpolation vector is computed by doing the difference between the internal coordinates of the S_0 minimum [Fig. 1(a)] and the coordinates of the corresponding conical intersection. The MS-CASPT2 energies of these crossings are included in Table I as well.

It is important to note that a radiationless decay through Ci1, Ci2, or Ci3 is a pure photophysical process. Such intersections will be only responsible for indirect reactions, that is, products would be formed in subsequent steps, for example, via Eq. (1). However, the surface hop at the Ci4 conical intersection can lead to deactivation of the S_3 state or to excited nitrosomethane [CH_3NO ($1\,^1A''$)] and excited oxygen [O (^1D)]. In order to reach the latter reaction path, a barrier of only 10 kcal/mol above Ci4 has to be surmounted. Figure 3(a) represents the MS-CASPT2 linear interpolation

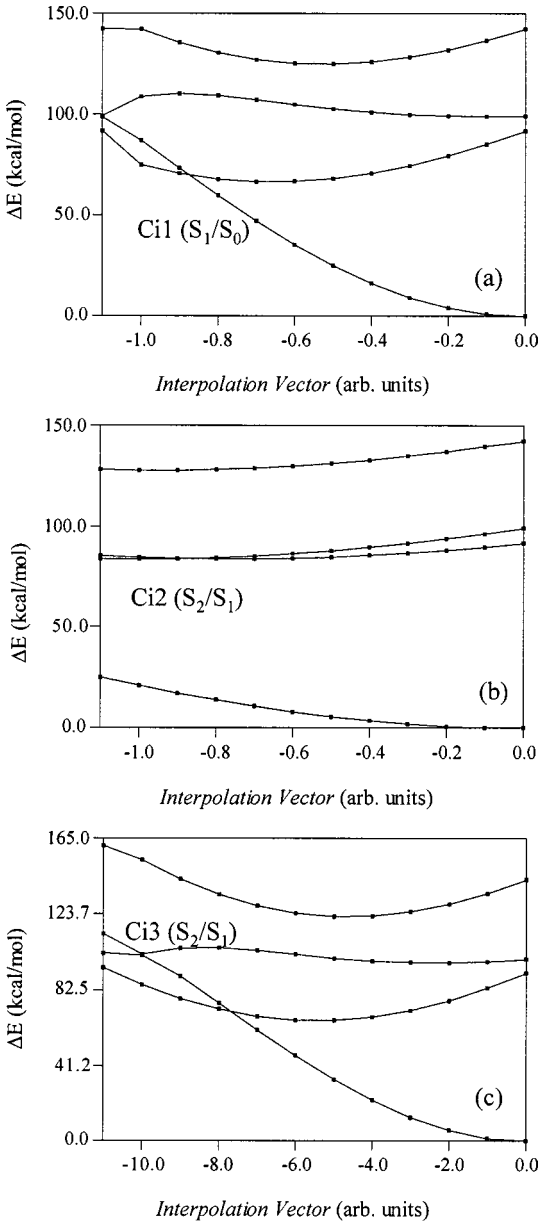

FIG. 2. Singlet MS-CASPT2/ANO-L linear interpolations (C_s symmetry). The geometry of the initial point corresponds to the S_0 minimum of nitromethane, the geometry of the end point corresponds to (a) S_1/S_0 conical intersection; (b) S_2/S_1 conical intersection; (c) S_2/S_1 (Ci3) conical intersection. Two roots have been included in each symmetry block for the MS-CASPT2 calculations.

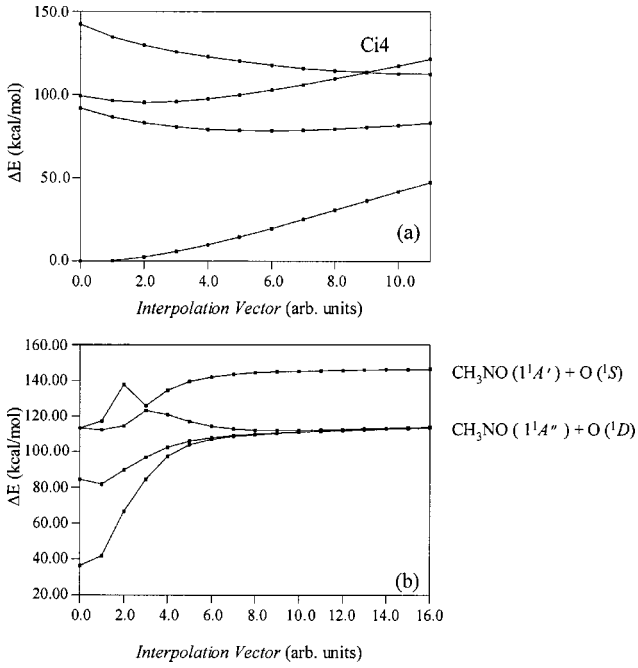

FIG. 3. Singlet MS-CASPT2/ANO-L linear interpolations (C_1 symmetry): (a) from the Franck–Condon point to the S_3/S_2 conical intersection; (b) from the S_3/S_2 conical intersection to dissociation into CH_3NO+O. Four roots have been included in the MS-CASPT2 calculations.

from the S_3 vertical point to Ci4 and Fig. 3(b) is the MS-CASPT2 interpolation which starts at Ci4 and leads to dissociation into CH_3NO ($1\,^1A''$) and O (^1D). The computed barrier for dissociation (10 kcal/mol) is, of course, lower than the vertical excitation energy at the starting point of the process. On the other hand, provided that nitrosomethane is generated in an excited state, decomposes easily into CH_3 ($1\,^2A_1'$) and NO ($X\,^2\Pi$), in fact, the transition state for dissociation of CH_3NO ($1\,^1A''$) is 8 kcal/mol above the CH_3NO ($1\,^1A''$) minimum, at the MS-CASPT2 level.

B. Triplet potential energy surfaces and intersystem crossings

On the triplet excited surfaces, the following stationary points have been localized: (i) on the T_1 (C_s) surface, a minimum [M3, Fig. 4(a)] and a second-order saddle point [TS_4, Fig. 4(b)] which leads to dissociation into CH_3 ($1\,^2A_1'$) and NO_2 ($1\,^2B_2$) [Dis1]; (ii) on the T_2 (C_s) surface, a first-order saddle point [Sd3, Fig. 4(c)] which is the lowest energy point on this surface and a first-order saddle point [TS_5, Fig. 4(d)] which is the transition state for dissociation into CH_3 ($1\,^2A_1'$) and NO_2 ($1\,^2A_2$) [Dis3]; and (iii) on the T_3 (C_s) surface, a minimum [M4, Fig. 4(e)] and a second-order saddle point [TS_6, Fig. 4(f)] which correlates adiabatically with the dissociation products CH_3 ($1\,^2A_1'$) and NO_2 ($1\,^2A_1$) [Dis0].

We have been able to localize the following lowest energy points in the seam of crossing of singlet and triplet surfaces: (a) T_1/S_0 intersystem crossing [Isc1, Fig. 4(g)]; (b) T_2/S_1 intersystem crossing [Isc2, Fig. 4(h)]; (c) T_3/S_1 intersystem crossing [Isc3, Fig. 4(i)]; and (d) T_4/S_2 intersystem crossing [Isc4, Fig. 4(j)]. Their MS-CASPT2 energies are collected in Table II. Figure 5 represents the MS-CASPT2 energy profiles of the singlet and triplet potential energy surfaces running from the S_0 minimum to Isc1, Isc2, and Isc3, respectively. In addition, the magnitude of the spin–orbit coupling constant along each interpolation is given in the same figure. These potential curves have been built according to the same criteria used in the construction of the interpolations corresponding to the conical intersections (Fig. 2, see above).

The energy profile of the T_4/S_2 crossing is represented in Fig. 6(a) along with the variation of the spin–orbit coupling constant in the interpolation coordinate, again the initial geometry corresponds to the S_0 minimum and the final one to Isc4. Figure 6(b) represents the potential curve for dissociation of Isc4 (T_4/S_2) into CH_3NO ($1\,^3A''$) and O (^1D).

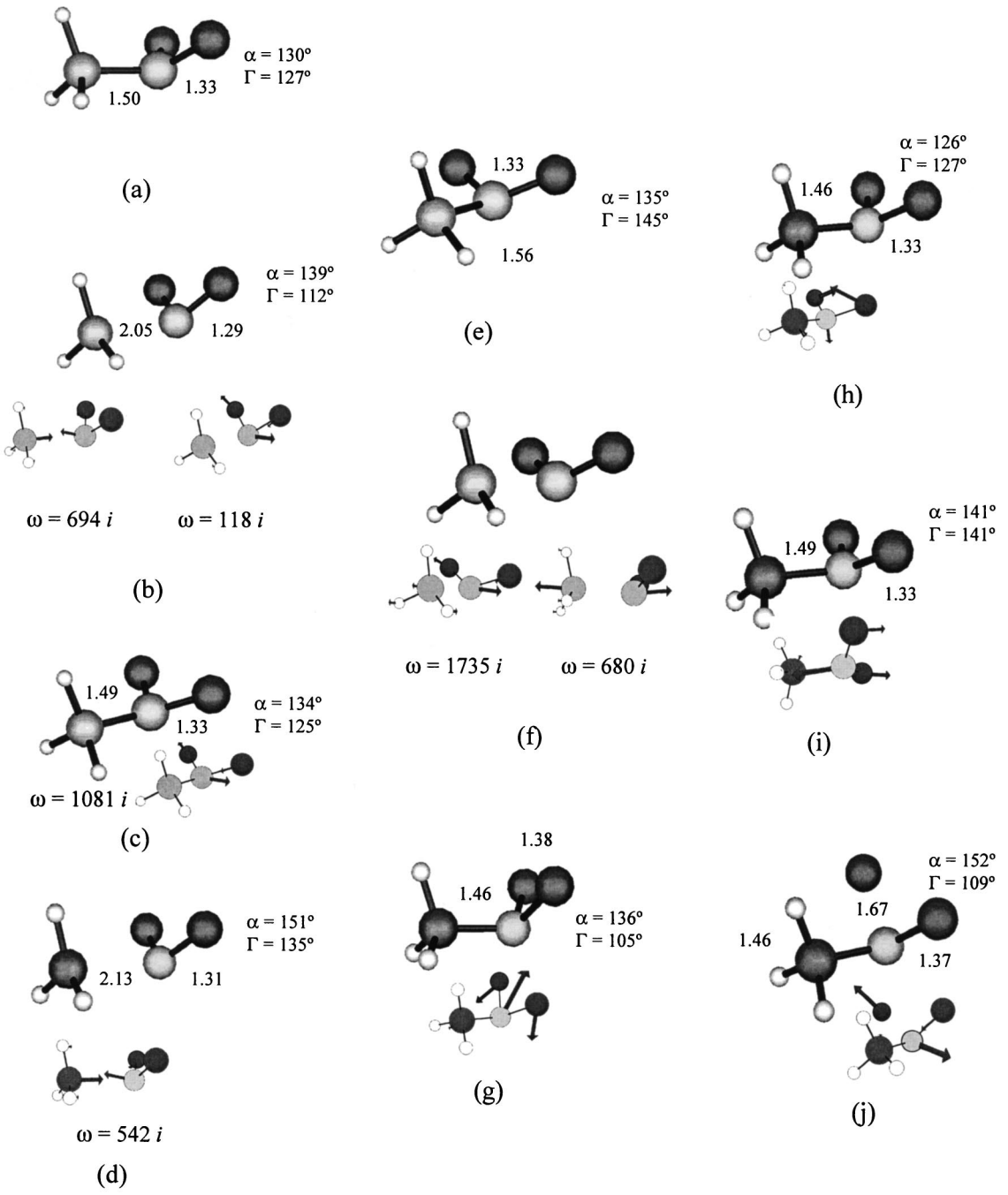

FIG. 4. Geometries of the critical points of nitromethane localized on the triplet surfaces at the CAS(14,11)/ANO-L level; intersystem crossings calculated at the CAS(14,10)/6-31G* level. The arrows in the lower structures correspond to imaginary modes (for stationary points) or gradient difference vectors (for intersystem crossings). (a) T_1, $1\,^3A''$ minimum; (b) T_1, $1\,^3A''$ transition state for dissociation into CH_3+NO_2 ($1B_2$); (c) T_2, $2\,^3A''$ first-order saddle point; (d) T_2, $2\,^3A''$ transition state for dissociation into CH_3+NO_2 ($1A_2$); (e) T_3, $1\,^3A'$ minimum; (f) T_3, $1\,^3A'$ transition state for dissociation into CH_3+NO_2 ($1A_1$); (g) T_1/S_0 intersystem crossing; (h) T_2/S_1 intersystem crossing; (i) T_3/S_1 intersystem crossing; and (j) T_4/S_2 intersystem crossing. Structures represented with the MACMOLPLT program (Ref. 42).

IV. DISCUSSION

We start our discussion of the reaction paths at the Franck–Condon point on the S_3 surface. To illustrate the following discussion, an energy-level diagram is shown in Fig. 7(a). The S_3 vertical point has three imaginary frequencies, the higher one (in absolute value) points to the S_3/S_2 crossing [Ci4, Fig. 1(l)], which, in turn, is the lowest energy point on the S_3 surface. On the other hand, the stationary structure depicted in Fig. 1(g) is a first-order saddle point (Sd2) with its imaginary mode pointing to the S_3/S_2 conical intersection as well. Hence, after excitation at 193 nm, the most plausible process is $S_3 \rightarrow S_2$ decay through the S_3/S_2 conical intersection, that is, the crossing region can be reached through two different routes: (1) direct, $S_3 \rightarrow$ Ci4; (2) indirect $S_3 \rightarrow$ Sd2 $\rightarrow$ Ci4. The actual paths will depend on the specific conditions in which the starting points are prepared. From this point of view, dissociation of excited nitromethane through TS_3 [Fig. 1(h)] to yield NO_2 ($1\,^2A_2$) is not very probable.

TABLE II. MS-CASPT2 energies of the critical points of nitromethane on the triplet surfaces. Zero point energy correction is included. Absolute reference energy, $E_h = -244.621\,23$ hartree.

Geometry	Configuration	ΔE (kcal/mol)	ZPE (kcal/mol)
M1a, S_0, $1\,^1A'$ [Fig. 1(a)]	$\cdots n\sigma(O)^2\sigma(CN)^2 n\pi(O)^2$	0.0 (0.00)[a]	3.2
Vt4, T_1, $1\,^3A''$	$\cdots n\sigma(O)^1\pi^*(NO)^1$	86.4 (3.75)	2.9
Vt5, T_2, $2\,^3A''$	$\cdots n\pi(O)^1\pi^*(NO)^1$	87.1 (3.78)	3.1
Vt6, T_3, $1\,^3A'$	$\cdots\sigma(CN)^1\pi^*(NO)^1$	94.8 (4.11)	2.9
M3, T_1, $1\,^3A''$ [Fig. 4(a)]	$\cdots n\pi(O)^1\pi^*(NO)^1$	62.1 (2.70)	3.0
TS4, T_1, $1\,^3A''$ [Fig. 4(b)]	$\cdots n\pi(O)^1\pi^*(NO)^1$	90.5 (3.92)	2.6
Sd3, T_2, $2\,^3A''$ [Fig. 4(c)]	$\cdots n\sigma(O)^1\pi^*(NO)^1$	68.8 (2.98)	2.9
TS5, T_2, $2\,^3A''$ [Fig. 4(d)]	$\cdots n\sigma(O)^1\pi^*(NO)^1$	114.0 (4.94)	2.6
M4, T_3, $1\,^3A'$ [Fig. 4(e)]	$\cdots\sigma(CN)^1\pi^*(NO)^1$	77.7 (3.37)	3.1
TS6, T_3, $1\,^3A'$ [Fig. 4(f)]	$\cdots\sigma(CN)^1\pi^*(NO)^1$	81.4 (3.53)	2.7
Isc1, T_1/S_0 [Fig. 4(g)][b]		64.3 (2.79)	…
Isc2, T_2/S_1 [Fig. 4(h)][b]		71.9 (3.12)	…
Isc3, T_3/S_1 [Fig. 4(i)][b]		74.7 (3.24)	…
Isc4, T_4/S_2 [Fig. 4(j)][b]		121.9 (5.29)	…
Dis5, $CH_3NO(1\,^3A'')+O(^1D)$[b]		114.0 (4.95)	…
Dis6, $CH_3NO(1\,^1A')+O(^3P)$[b]		100.1 (4.34)	…

[a]In parenthesis energy in eV.
[b]Zero point energy correction not included.

Once the S_3/S_2 surface hop has taken place, four reaction channels are open on the S_2 surface: (1) dissociation through TS_2 to give $NO_2(1\,^2B_1)$; (2) dissociation into $CH_3NO(1\,^1A'')$ and $O(^1D)$; (3) radiationless decay to S_1 through the S_2/S_1 conical intersection [Ci2, Fig. 1(j)]; and (4) radiationless decay to S_0 through the S_2/S_1 conical intersection [Ci3, Fig. 1(k)]. As it will be illustrated in the next paragraph, the most probable routes are (2) and (3).

For a polyatomic molecule with *n* internal degrees of freedom, a conical intersection arises when two electronic states of the same multiplicity cross. For such a situation, if the energy of these two states is plotted against two special directions or vectors, a figure of double cone is obtained.[34] These vectors are the so-called gradient difference (GD) and nonadiabatic coupling (NAC) vectors. In contrast, the energy degeneracy remains for the other *n*-2 internal degrees of freedom, which in turn, are orthogonal to the plane spanned by the GD and NAC vectors.

The existence of a conical intersection has important dynamical consequences: (i) very efficient radiantionless decay from the upper to the lower state becomes possible at this point; (ii) the existence of this topological figure provides access to a limited number of pathways that can lead to different photoproducts. As the system enters the region of the conical intersection, its momentum will be orientated in the direction of the pathway which is approximately parallel to vector GD. After the surface hop, the trajectories of the molecules will follow the direction of GD only if they pass exactly through the tip of the cone.[35,36] However, most of the trajectories will miss the cone tip; in this case, an amount of energy equal to the height of the jump will be distributed along NAC according to Tully and Preston.[37] Thus, after the surface jump, the initial direction of motion will be determined by combination of the original momentum on the upper state with this second component along NAC, that is, the system will evolve on the plane spanned by these two vectors.

The plane defined by the nonadiabatic coupling vector and gradient difference vector of Ci4 represented in Fig. 1(l) spans both the domain of the S_2/S_1 [Ci2, Fig. 1(j)] conical intersection (or S_2 minimum) and oxygen extrusion. So that, it seems rather clear from the preceding discussion in the above paragraph that the most probable routes after the S_3/S_2 hop are (i) S_2/S_1 radiationless decay and (ii) dissociation into CH_3NO $(1\,^1A'')+O$ (^1D) [channel (2)]. In addition, if S_2/S_1 surface hop does not happen, then the S_2 minimum region is populated. It allows an efficient intramolecular vibrational redistribution; thereafter it is possible either radiationless decay to S_0 via the S_2/S_1 (Ci3) conical intersection [channel (3)] or dissociation into CH_3 and NO_2 $(1\,^2B_1)$ [channel (4)], both reaction paths have almost the same energy barrier.

After the S_2/S_1 [Ci2, Fig. 1(j)] jump, the momentum of the molecule is again partitioned into the directions of the NAC and GD vectors, that is, the system is directed either to a new surface crossing [Ci1 (S_1/S_0), Fig. 1(i)] or to the S_1 minimum of C_1 symmetry, which is the global minimum on the S_1 surface, and then it dissociates into CH_3 $+NO_2$ $(1\,^2B_2)$.

Once the system has reached the S_0 state through Ci1, it has accumulated enough internal energy to dissociate into CH_3 and NO_2 $(1\,^2A_1)$. It must be pointed out that this $1\,^2A_1$ state must correspond to an excited state and not to the ground state of NO_2, in fact, it is well known that the A_1 and B_2 states of NO_2 cross along a C_{2v} path.[38] This hypothesis is supported by the agreement between the lifetime (25 μs) estimated by ourselves for the $A_1 \rightarrow B_2$ transition and a value of 35 μs reported by Butler *et al.*[7] in the fluorescence emission detected in the photodissociation of nitromethane at 193 nm. In contrast, the computed lifetime of the B_2 state is two orders of magnitude lower (0.2 μs). Therefore, it seems clear from the preceding discussion that nitrogen dioxide is mainly formed in two electronically excited states, $1\,^2B_1$ and $1\,^2A_1^*$.

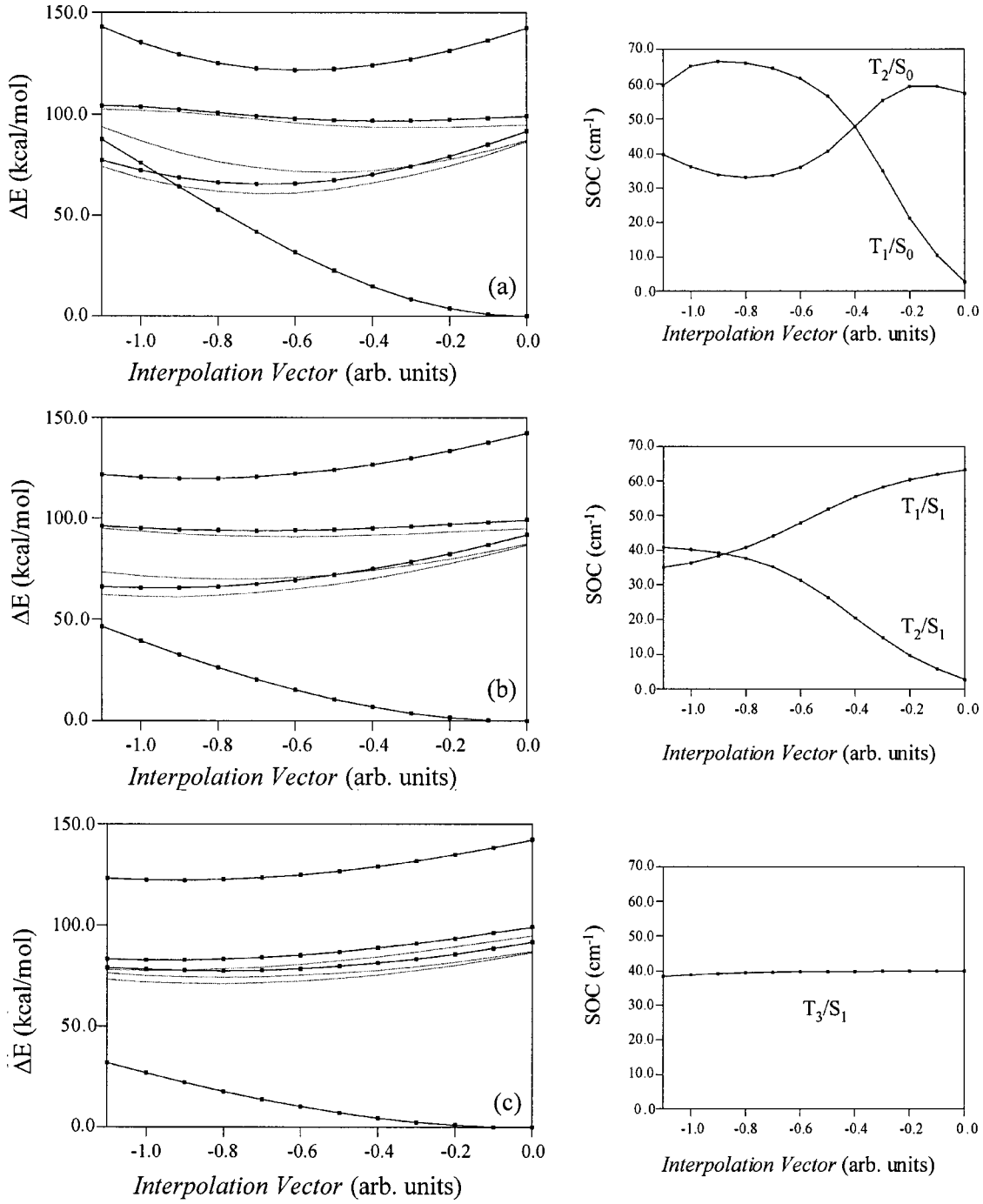

FIG. 5. Singlet and triplet MS-CASPT2/ANO-L linear interpolations (C_s symmetry). The geometry of the initial point corresponds to the S_0 minimum of nitromethane, and the geometry of the end point corresponds to (a) T_1/S_0 intersystem crossing; (b) T_2/S_1 intersystem crossing; (c) T_2/S_1 intersystem crossing. Two roots have been included in each symmetry block for the MS-CASPT2 calculations, excepting the T_3 state which has been computed using one root. The lower graphics at the right of each principal figure represent the magnitude of the spin–orbit coupling constants along the respective interpolation curve.

An important experimental observation made in the 193 nm photolysis of nitromethane is the formation of nitric oxide in an excited state [NO ($A\,^2\Sigma$)].[10] We must conclude that NO ($A\,^2\Sigma$) cannot arise from any excited state of NO_2, because at 193 nm there are no resonant transitions of any state of NO_2 which in a subsequent dissociation path could yield excited nitric oxide. Of course, at this wavelength there are several resonant transition of NO_2 corresponding to different electronic excited states, but they would be only responsible for generation of NO ($X\,^2\Pi$). Hence, the only available source of excited nitric oxide is an excited state of nitrosomethane. This species would yield NO in its ground electronic state if it is excited in either of the two lowest states, S_0 or S_1. In order to form excited nitric oxide, the populated state must be the third excited state or even higher. In fact, there are two almost resonant transitions of the S_1 state ($1A''$) with the excitation light at 193 nm. They correspond to the $1A'' \rightarrow 3A'$ and $1A'' \rightarrow 3A''$ transitions, respectively, and the computed vertical energies amount to 179 and 187 nm with oscillator strengths of 0.28×10^{-4} and 0.92×10^{-3}. On the other hand, the barrier height for the reaction CH_3NO ($1\,^1A'') \rightarrow CH_3 + NO$ ($X\,^2\Pi$) is only 8 kcal/mol at the

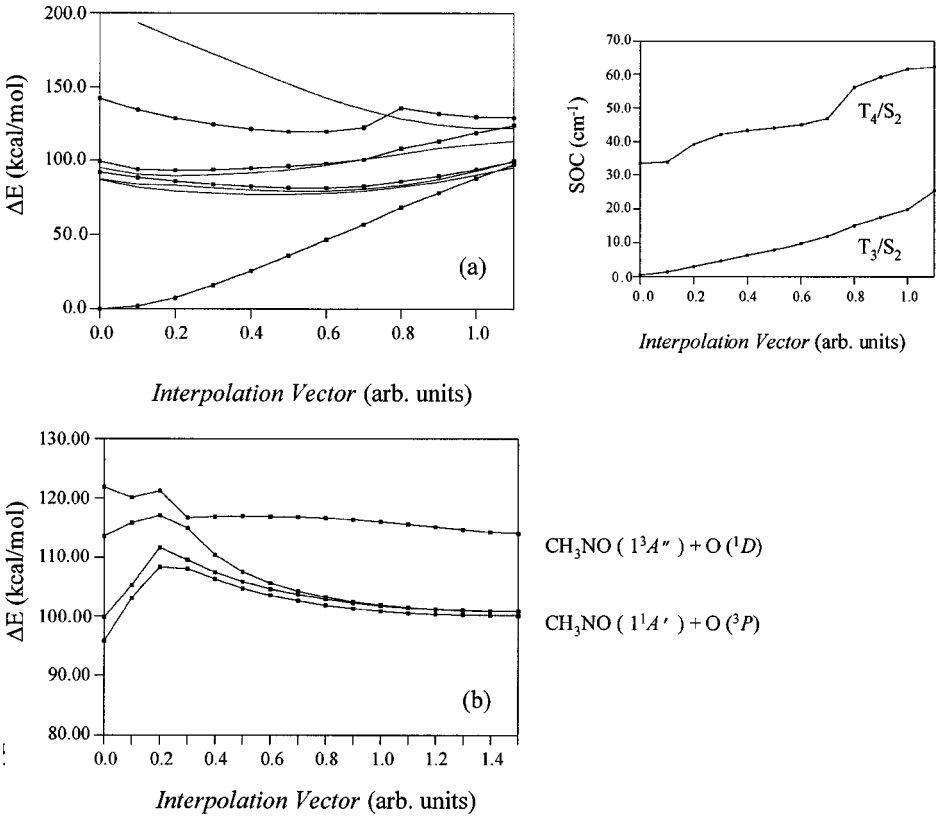

FIG. 6. MS-CASPT2/ANO-L linear interpolations (C_1 symmetry): (a) from the Franck–Condon point to the T_4/S_2 intersystem crossing; (b) from the T_4/S_2 intersystem crossing to dissociation into CH_3NO+O. Four roots have been included in the MS-CASPT2 calculations.

MS-CASPT2 level. Therefore, nitrosomethane formed in channel (2) will not survive enough to get to at the detector.

To finish, we discuss the triplet surfaces whose energy-level diagram is shown in Fig. 7(b). As it was pointed above, four intersystem crossings have been localized: T_1/S_0 [Isc1, Fig. 4(g)], T_2/S_1 [Isc2, Fig. 4(h)], T_3/S_1 [Isc3, Fig. 4(i)], and T_4/S_2 [Isc4, Fig. 4(j)]. In each case, they have been optimized as the lowest energy point in the seam of crossing of the singlet and triplet surfaces.

The analysis of the role of intersystem crossing in the dynamics of a process is not at all an easy task. To describe intersystem crossing processes quantitatively, one needs not only the potential surfaces involved and spin–orbit couplings as functions of coordinate, but also dynamics methods that are capable of describing coupled surfaces where multiple intersections are possible.[39] For example, recently, Schatz and co-workers[39,40] have proposed a methodology to study intersystem crossing process (ISC) effects which is based upon a quasiclassical trajectory surface-hopping method to determine dynamical information based on a diabatic representation. Unfortunately, this method is applicable only to atom-diatom and related chemical reactions.

In what follows, we will be content with a qualitative description of the ISC processes involved in the photodynamics of nitromethane. In principle, the crossings Isc2 and Isc3 can be ruled out because two conical intersections (Ci1 and Ci2) coexist with such intersystem crossings, that is, these conical intersections are very close to the singlet-triplet crossings both structurally and energetically (see Figs. 1 and 4; Tables I and II). Hence, it is likely that internal conversion is more efficient than intersystem crossing.

A different situation would arise for the $S_0 \rightarrow T_1$ crossing. To estimate the probability of an intersystem crossing process P^{ISC}, a modified Landau–Zener model can be applied,[41] Eq. (6);

$$P^{\mathrm{ISC}} = 1 - \exp\left(- \frac{\pi}{4} \frac{8\langle \Psi_I^0 | \hat{H}_{\mathrm{SO}} | \Psi_J^0 \rangle^2}{\sum_\alpha g_\alpha^{\mathrm{IJ}} \mathrm{v}_\alpha} \right) \tag{6}$$

where $\langle \Psi_I^0 | \hat{H}_{\mathrm{SO}} | \Psi_J^0 \rangle$ is the magnitude of the spin–orbit coupling constant defined in Eq. (5), g_α is the gradient of the energy difference, and v_α is the nuclear velocity.

Equation (6) shows how the intersystem crossing probability depends on the spin–orbit coupling, the nuclear velocity and the local topology of the potential energy surfaces (through g_α). Provided that the crossing Isc1 (T_1/S_0) occurs at the immediacy of a turning point [Fig. 5(a)], the velocity of the nuclei must be low enough at this region. In addition, we have computed a rather large spin–orbit coupling constant and similar energy gradient difference between both states. Consequently, a high probability P^{ISC} is expected for Isc1. The same reasoning is applied to Isc4 (T_4/S_2). At the immediacy of (T_4/S_2) there are two factors which favor the $S_2 \rightarrow T_4$ jump: (1) the relative large magnitude of the spin–orbit coupling constant [Fig. 6(b)]; and (2) the topology of the S_2 potential energy surface [Fig. 6(a)] in the vicinity of the lowest energy point in the seam of crossing corresponds to a turning point where the velocity of the nuclei approaches to zero. Thus, if the $S_2 \rightarrow T_4$ jump occurs, then $O(^1D)$ and CH_3NO ($1\,^3A''$) will be formed after the crossing [Fig. 6(c)]. Although, due to the low barrier for dissociation of triplet nitrosomethane, CH_3+NO ($X\,^2\Pi$) would be the observed products.

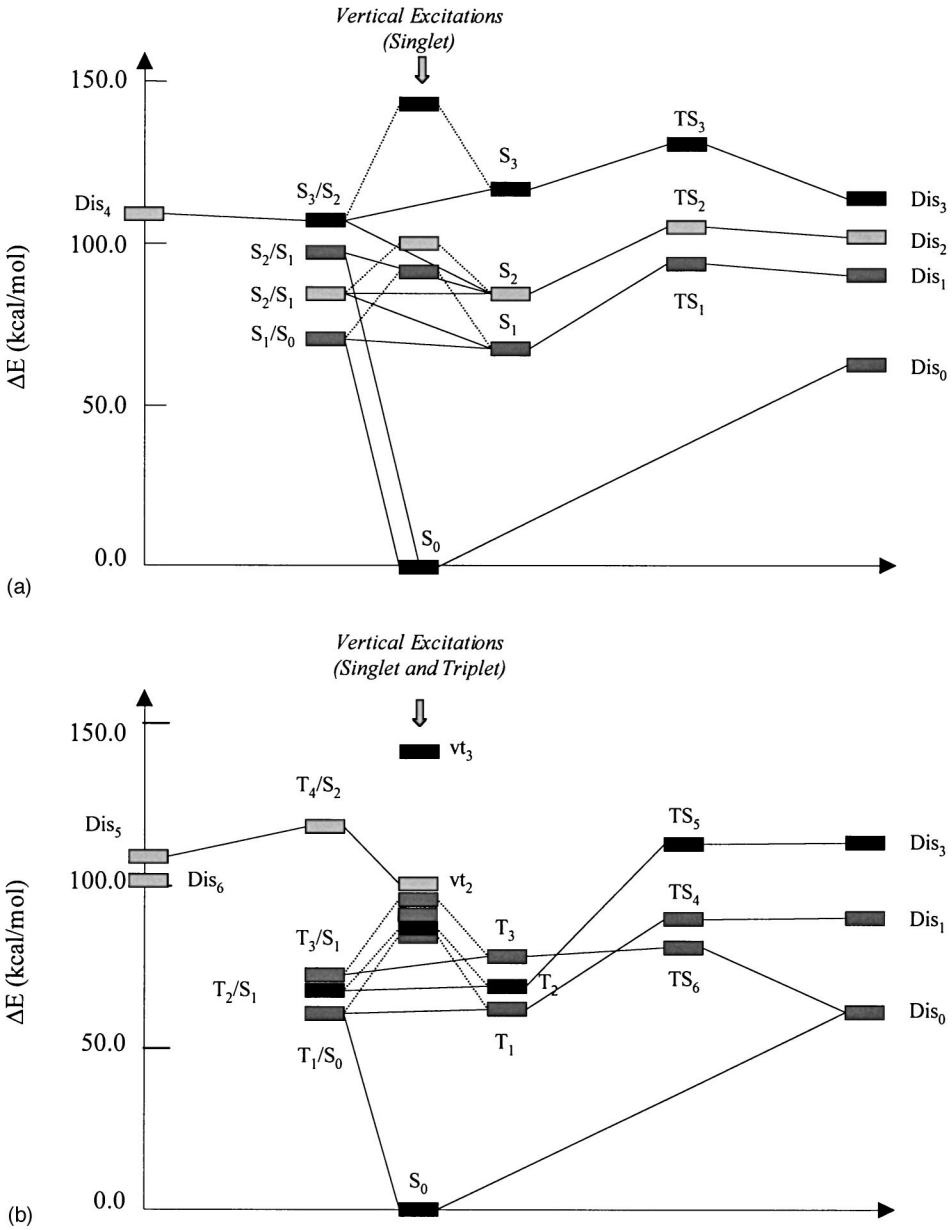

FIG. 7. Energy-level diagrams of all of the critical points involved in the photochemistry of nitromethane. (a) Single states. (b) Triplet states.

V. SUMMARY

It is found that the key step in the photodissociation dynamics of nitromethane is the radiationless decay through the S_3/S_2 conical intersection [Ci4, Fig. 1(i)]:

$$CH_3NO_2(1\,^1A',S_0) + h\upsilon(193\text{ nm}) \rightarrow CH_3NO_2(2\,^1A'',S_3) \rightarrow Ci4(S_3/S_2). \quad (7)$$

Thereafter, the following reaction paths are accessible:

$$\text{(a) } Ci4(S_3/S_2) \rightarrow CH_3NO(1\,^1A'',S_1) + O(^1D), \quad (8)$$

$$\text{(b) } Ci4(S_3/S_2) \rightarrow Ci2(S_2/S_1) \rightarrow CH_3NO(S_1) \rightarrow CH_3 + NO_2(1\,^2B_2), \quad (9)$$

$$\text{(c) } Ci4(S_3/S_2) \rightarrow Ci2(S_2/S_1) \rightarrow Ci1(S_1/S_0) \rightarrow CH_3NO_2(S_0) \rightarrow CH_3 + NO_2(1\,^2A_1)^*, \quad (10)$$

where the asterisk on NO_2 means that it is generated in an electronic excited state.

In addition, the formation of excited nitric oxide is explained by absorption of a second photon:

$$\text{(d) } CH_3NO(1\,^1A'') + h\upsilon(193\text{ nm}) \rightarrow CH_3 + NO(A\,^2\Sigma). \quad (11)$$

Reaction (11) does not preclude a secondary absorption by NO_2, however, such an absorption would be responsible for NO ($X\,^2\Pi$) yielding. On the other hand, NO_2 produced in channels (9) and (10) may decompose into NO ($X\,^2\Pi$) $+O(^3P)$ in a subsequent reaction provided that NO_2 is generated in both cases as a hot molecule.

Finally, we want to make some comments about the crossings localized at the MS-CASPT2 level. We can only check that they are actual conical intersections at the CASSCF level by examining the gradient of the upper state in each case and so we did. Moreover it is reasonable to think that they will still behave as crossing points and not as avoided intersections at the MS-CASPT2 level. Ci1 and Ci3 have C_s symmetry and the interacting states belong to different irreducible representations, so that, each of the interpolations on these points could be performed keeping the C_s symmetry. Consequently, each potential energy surface is computed and followed independently what allows a unequivocal localization of the crossing point at the MS-CASPT2 level. The most problematic point could be Ci4, which corresponds to a molecular arrangement with C_1 symmetry. However, the structures found by the CAS-SCF and MS-CASPT2 for this degenerate point are very close. Furthermore, the energy difference between the touching surface amounts only to 0.29 kcal/mol at the MS-CASPT2 level. Therefore, it can be reasonably expected that it is a real crossing at the MS-CASPT2 level as well.

ACKNOWLEDGMENT

This research was supported by the Spanish Ministerio de Ciencia y Tecnologia (Project No. BQU2003-1453).

[1]H. S. Kilic, K. W. D. Ledingham, C. Kosmidis *et al.*, J. Phys. Chem. A **101**, 817 (1997).
[2]M. R. Manaa, E. J. Reed, L. E. Fried, G. Galli, and F. Gygi, J. Chem. Phys. **120**, 10146 (2004).
[3]A. Pelc, W. Sailer, S. Matejcik, P. Scheier, and T. D. Märk, J. Chem. Phys. **119**, 7887 (2003).
[4]F. I. Bellisarii, S. Gallina, M. Zimarino, and R. De Caterina, Eur. J. Clin. Invest **33**, 933 (2003).
[5]I. C. Walker and M. A. D. Fluendy, Int. J. Mass. Spectrom. **205**, 171 (2001).
[6]J. F. Arenas, J. C. Otero, D. Peláez, and J. Soto, J. Chem. Phys. **119**, 7814 (2003).
[7]L. J. Butler, D. Krajnovich, Y. T. Lee, G. Ondrey, and R. Bersohn, J. Chem. Phys. **79**, 1708 (1983).
[8]N. C. Blais, J. Chem. Phys. **79**, 1723 (1983).
[9]K. Q. Lao, E. Jensen, P. W. Kash, and L. J. Butler, J. Chem. Phys. **93**, 3958 (1990).
[10]D. B. Moss, K. A. Trentelman, and P. L. Houston, J. Chem. Phys. **96**, 237 (1992).
[11]K. J. Spears and S. P. Brugge, Chem. Phys. Lett. **54**, 373 (1978).
[12]P. E. Schoen, M. J. Marrone, J. M. Schnur, and L. S. Goldberg, Chem. Phys. Lett. **90**, 272 (1981).
[13]S. Zabarnick, J. W. Fleming, and A. P. Baronavski, J. Chem. Phys. **85**, 3395 (1986).
[14]G. D. Greenblatt, H. Zuckermann, and Y. Hass, Chem. Phys. Lett. **134**, 593 (1986).
[15]C. Rajchenbach, G. Jonusauskas, and C. Rullière, Chem. Phys. Lett. **231**, 467 (1994).
[16]S. Paszyc, J. Photochem. **2**, 183 (1973).
[17]K. Honda, H. Mikuni, and M. Takahasi, Bull. Chem. Soc. Jpn. **45**, 3534 (1972).
[18]W. D. Taylor, T. D. Allston, M. J. Moscato, G. B. Fazekas, R. Kozlowski, and G. A. Takas, Int. J. Chem. Kinet. **12**, 231 (1980).
[19]M. S. Park, K.-H. Jung, H. P. Upadhyaya, and H.-R. Volpp, Chem. Phys. **270**, 133 (2001).
[20]P.-O. Widmark, P.-Å. Malmqvist, and B. O. Roos, Theor. Chim. Acta **77**, 291 (1990).
[21]B. O. Roos, in *Advances in Chemical Physics*, Ab Initio Methods in Quantum Chemistry Vol. 2, edited by K. P. Lawley (Wiley, Chichester, United Kingdom, 1987), Chap. 69, p. 399.
[22]K. Andersson, M. Barysz, A. Bernhardsson *et al.*, MOLCAS, version 5.4. (Lund University, Sweden, 2002).
[23](a) M. J. Frisch, G. W. Trucks, H. B. Schlegel *et al.*, GAUSSIAN 03, Revision B.04, Gaussian, Inc., Pittsburgh, PA, 2003; (b) M. J. Bearpark, M. A. Robb, and H. B. Schlegel, Chem. Phys. Lett. **223**, 269 (1994); (c) D. R. Yarkony, J. Chem. Phys. **92**, 2457 (1990).
[24]J. F. Arenas, S. P. Centeno, I. López-Tócon, D. Peláez, and J. Soto, J. Mol. Struct.: THEOCHEM **630**, 17 (2003).
[25]J. F. Arenas, J. C. Otero, D. Peláez, J. Soto, and L. Serrano-Andrés, J. Chem. Phys. **121**, 4127 (2004).
[26]J. F. Arenas, J. I. Marcos, I. López-Tócon, J. C. Otero, and J. Soto, J. Chem. Phys. **113**, 2282 (2000).
[27]J. Finley, P.-Å. Malmqvist, B. O. Roos, and L. Serrano-Andrés, Chem. Phys. Lett. **288**, 299 (1998).
[28]N. Forsberg and P.-Å. Malmqvist, Chem. Phys. Lett. **274**, 196 (1997).
[29]P.-Å. Malmqvist, Int. J. Quantum Chem. **30**, 470 (1986); P.-Å. Malmqvist and B. O. Roos, Chem. Phys. Lett. **155**, 189 (1989).
[30]B. A. Hess, C. Marian, U. Wahlgren, and O. Gropen, Chem. Phys. Lett. **251**, 365 (1996).
[31]P.-Å. Malmqvist, B. O. Roos, and B. Schimmelpfenning, Chem. Phys. Lett. **357**, 230 (2002).
[32]C. Ribbing, B. Gilliams, K. Pierloot, B. O. Roos, and G. Karlström, J. Chem. Phys. **109**, 3145 (1998).
[33]T. R. Furlani and H. F. King, J. Chem. Phys. **82**, 5577 (1985).
[34]E. Teller, J. Phys. Chem. **41**, 109 (1937).
[35]M. Klessinger and J. Michl, *Excited States and Photochemistry of Organic Molecules* (WCH, New York, 1995).
[36]J. F. Arenas, I. López-Tocón, J. C. Otero, and J. Soto, J. Am. Chem. Soc. **124**, 1728 (2002).
[37]J. C. Tully and R. K. Preston, J. Chem. Phys. **55**, 562 (1971); J. C. Tully, *ibid.* **93**, 1061 (1990).
[38]E. R. Davidson and W. T. Borden, J. Phys. Chem. **87**, 4783 (1983).
[39]B. Maiti and G. C. Schatz, J. Chem. Phys. **119**, 12360 (2003).
[40]M. R. Hoffmann and C. Schatz, J. Chem. Phys. **113**, 9456 (2000).
[41]D. R. Yarkony, J. Am. Chem. Soc. **114**, 5406 (1992).
[42]B. M. Bode and M. S. Gordon, J. Mol. Graphics Modell. **16**, 133 (1999).